

Entanglement evolution after connecting finite to infinite quantum chains

V. Eisler¹, D. Karevski², T. Platini² and I. Peschel¹

¹ Fachbereich Physik, Freie Universität Berlin, Arnimallee 14, D-14195 Berlin, Germany

² Laboratoire de Physique des Matériaux, UMR CNRS 7556, Université Henri Poincaré, Nancy 1, B.P. 239, F-54506 Vandoeuvre-les-Nancy Cedex, France

Abstract. We study zero-temperature XX chains and transverse Ising chains and join an initially separate finite piece on one or on both sides to an infinite remainder. In both critical and non-critical systems we find a typical increase of the entanglement entropy after the quench, followed by a slow decay towards the value of the homogeneous chain. In the critical case, the predictions of conformal field theory are verified for the first phase of the evolution, while at late times a step structure can be observed.

1. Introduction

The complexity of many-body quantum states manifests itself in the connection between different parts of a system in the wave function. It can be measured by the entanglement entropy S which has been studied extensively over the last years and shows, for example, a logarithmic divergence at quantum phase transitions in chains [1]. More recently, its temporal evolution for evolving quantum states has come into the focus of the studies. The simplest situation is a quench, where the Hamiltonian is changed instantaneously from H_0 to H_1 and one follows the subsequent evolution of the initial state, usually taken to be the ground state of H_0 . The first such studies considered global quenches, in which a parameter is changed everywhere in the same way [2, 3]. It was found that in this case the entanglement entropy becomes extensive, in contrast to the equilibrium states where it is proportional to the interface area between the two chosen parts of the system.

A different situation is that of a local quench, where a parameter is changed only in one or in a few places. For example, a single nearest-neighbour bond could be modified. In one dimension, this can have strong effects, since by removing or adding the full bond, one cuts the chain or joins previously separate pieces. In the first case, the initial entanglement is conserved, but in the second case it shows interesting temporal behaviour. This was investigated recently in a numerical study of free electrons hopping on a chain with initially one defect in form of a weakened bond which was then removed [4]. In spin language, this corresponds to an XX model. The entanglement entropy

was found to increase to a maximum, or plateau, followed by a slow decay to its equilibrium value. The maximum value was proportional to $\ln L$, where L is the size of the chosen subsystem, and the whole plateau could be described by a logarithmic expression containing L and the elapsed time t . In a subsequent publication, Calabrese and Cardy [5] showed how to obtain such plateaus and the corresponding formulae from conformal field theory. They also found that the long-time tails in S are absent in this continuum treatment and must therefore be lattice effects.

In the present study we continue these investigations by looking at chains where a finite segment is initially fully separated from the rest and then joined to it. This can be done on one or on both sides of the segment and the rest is assumed to be infinite. All parts of the total system are initially in their ground states. As examples we consider the XX model and the transverse Ising (TI) model for which the entanglement can be obtained in a relatively simple way from the correlation functions. This is outlined in the following section 2. The critical case is then studied in section 3. As for the single defect, we find logarithmic plateaus for $S(t)$ which turn out to be in very good agreement with conformal predictions. For the doubly-infinite geometry we derive the corresponding formula by extending the treatment in [5]. We also illustrate how the entanglement process manifests itself via fronts in the eigenvectors of the reduced density matrix and show the evolution of the single-particle spectra underlying S . An interesting new phenomenon appears in the long-time behaviour of $S(t)$, where one finds a step structure in the slow decay towards equilibrium. The non-critical case is investigated for the TI model in Section 4. Here we find a plateau in S as well, but with a flat shape (up to oscillations) and a limited height depending on the transverse field. Our findings are summarized in Section 5. Two appendices treat the relation between the entanglement entropies of the XX and the critical TI model and the derivation of the conformal formula for one of the geometries.

2. Models and geometries

In the following we study the XY quantum chain with Hamiltonian

$$H = -\frac{1}{2} \sum_{n=1}^{N-1} \left[\frac{1+\kappa}{2} \sigma_n^x \sigma_{n+1}^x + \frac{1-\kappa}{2} \sigma_n^y \sigma_{n+1}^y \right] - \frac{h}{2} \sum_{n=1}^N \sigma_n^z, \quad (1)$$

where the σ_n^α are Pauli matrices, for two special cases, namely

- $\kappa = h = 0$ which is the XX chain, critical and equivalent to a half-filled electronic hopping model
- $\kappa = 1$ which is the Ising chain in a transverse field.

As is well known, the operator H becomes a quadratic form when expressed in terms of Fermi operators c_n, c_n^\dagger and reads after diagonalization

$$H = \sum_q \omega_q \left(\eta_q^\dagger \eta_q - 1/2 \right) \quad (2)$$

with

$$\omega_q = \sqrt{\kappa^2 \sin^2 q + (h + \cos q)^2}. \quad (3)$$

In general, the η_q are obtained from the c_n, c_n^\dagger via a Bogoliubov transformation with two sets $\phi_q(n), \psi_q(n)$ of coefficients [6]. For the XX case this reduces to a simple linear combination of the c_n and one can also write H as

$$H_{XX} = - \sum_q \cos q \eta_q^\dagger \eta_q \quad (4)$$

with $q = \pi n / (N + 1), n = 1, 2, \dots, N$ for open boundary conditions.

We will investigate the two situations depicted in Fig. 1. In the first case the system consists initially of a segment of length L and a rest of length $N - L$ where $N \gg L$, both of which are in their ground state. We will call this the semi-infinite geometry. In the second case, the segment is sandwiched between two such environments. This will be called the infinite geometry. At time $t = 0$, the missing bond(s) will be added and the time evolution of the state monitored.

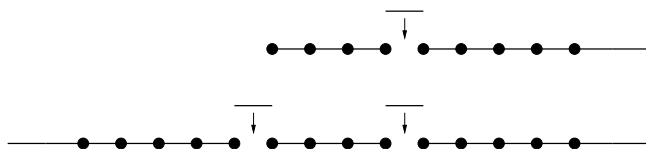


Figure 1. The two geometries studied in the paper.

We will be interested in the entanglement of the segment with the rest of the system. The corresponding entanglement entropy S follows from the reduced density matrix ρ of the segment which has the form [7]

$$\rho = \frac{1}{Z} e^{-\mathcal{H}}, \quad \mathcal{H} = \sum_{k=1}^L \varepsilon_k(t) f_k^\dagger f_k \quad (5)$$

Here Z is a normalization constant ensuring $\text{Tr} \rho = 1$ and the fermionic operators f_k follow from the c_n by an orthogonal transformation. Then $S = -\text{Tr}(\rho \ln \rho)$ is determined by the single-particle eigenvalues $\varepsilon_k(t)$ according to

$$S(t) = - \sum_k \zeta_k(t) \ln \zeta_k(t) - \sum_k (1 - \zeta_k(t)) \ln(1 - \zeta_k(t)), \quad (6)$$

where $\zeta_k(t) = 1 / (\exp(\varepsilon_k(t)) + 1)$.

Since the initial state is a Slater determinant, the $\varepsilon_k(t)$ resp. the $\zeta_k(t)$ follow from the one-particle correlation functions at time t . These can be combined into a $2N \times 2N$ matrix

$$\mathbf{G} = \begin{pmatrix} \langle \Gamma_m^1 \Gamma_n^1 \rangle & \langle \Gamma_m^1 \Gamma_n^2 \rangle \\ \langle \Gamma_m^2 \Gamma_n^1 \rangle & \langle \Gamma_m^2 \Gamma_n^2 \rangle \end{pmatrix} \quad (7)$$

where $\Gamma_n^1 = (c_n^\dagger + c_n)$ and $\Gamma_n^2 = -i(c_n^\dagger - c_n)$. Restricting this matrix to the L sites in the subsystem, its eigenvalues are ζ_k and $1 - \zeta_k$. In the XX case, it is sufficient to consider the $N \times N$ correlation matrix

$$\mathbf{C} = \langle c_m^\dagger c_n \rangle \quad (8)$$

which has eigenvalues ζ_k when restricted to the subsystem.

The time evolution of the fermionic operators with the final Hamiltonian gives the correlation matrix at time t in terms of its initial value as [8, 9]

$$\mathbf{G}(t) = \mathbf{R}(t)\mathbf{G}(0)\mathbf{R}^T(t) \quad (9)$$

where $\mathbf{R}(t)$ is a rotation matrix with elements which are sums containing the $\phi_q(n), \psi_q(n)$ and exponential factors $\exp(i\omega_q t)$. In the critical case and taking the thermodynamic limit, they can be expressed in terms of Bessel functions. The initial correlations are particularly simple for the XX model, where one finds for a segment with sites between 1 and L

$$C_{ij} = \frac{1}{2(L+1)} \left[\frac{\sin(\frac{\pi}{2}(i-j))}{\sin(\frac{\pi}{2(L+1)}(i-j))} - \frac{\sin(\frac{\pi}{2}(i+j))}{\sin(\frac{\pi}{2(L+1)}(i+j))} \right] \quad (10)$$

It was shown recently that in the ground state there is a close connection between the entanglement entropies of the XY chain with $h = 0$ and the TI chain [10]. The consideration can be extended to the time-dependent case as sketched in Appendix A and gives at criticality

$$S_{XX}(L, t) = 2 S_{TI}(L/2, t/2) \quad (11)$$

One can see this relation clearly in numerical computations of S . For the spectra it means that the same ε_k occur in both systems, which one can also verify numerically. In the critical case we will therefore only present results for the XX model. These were obtained by determining $C_{ij}(t)$ in the subsystem by summing Bessel functions as in [4]. For the non-critical case we will consider the TI model. Here the procedure was to calculate the full correlation matrix $\mathbf{G}(t)$ from $\mathbf{G}(0)$ for a sufficiently large total system using (9) and then to specialize to the subsystem. The size was chosen such that reflection phenomena in the larger subsystem could not yet enter the dynamics.

3. Critical chains

General behaviour

The general behaviour of the entanglement entropy is shown in Fig. 2 and can be described as follows. Starting from the value $S(0) = 0$ (since the subsystems are separated initially), it rises quickly to a broad plateau which extends to the times $t = 2L$ in the semi-infinite and $t = L$ in the infinite geometry, respectively. Afterwards it decreases slowly to its equilibrium value. The characteristic times are those an excitation with the maximum velocity $v_F = 1$ needs in order to travel from the initial gap to the end of the segment. In the semi-infinite case this involves a reflection at the boundary, which gives $t = 2L$.

Such a propagation phenomenon is clearly visible in the eigenvectors of the single-particle states of ρ . Fig. 3 shows the lowest one for four different times and both geometries. In the semi-infinite case (left side) one sees a front propagating from the initial defect towards the end where it is reflected. For the infinite geometry (right

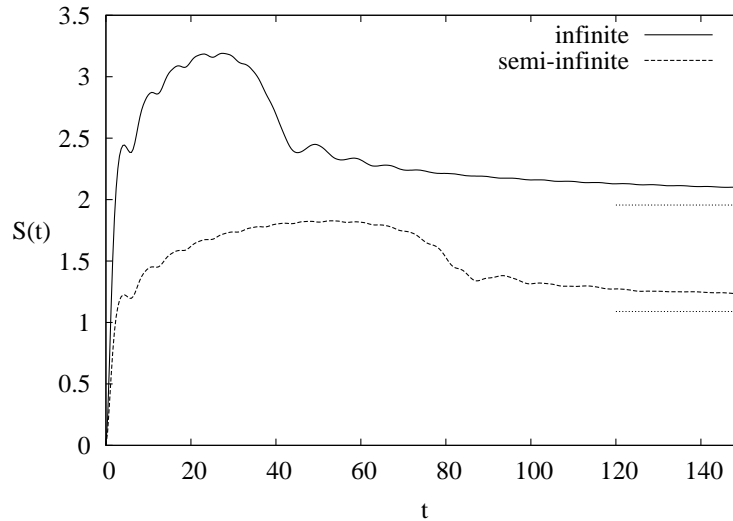


Figure 2. Entanglement entropy for $L = 40$ and both geometries. The dotted lines on the right are the corresponding equilibrium values.

side) one has two fronts propagating inwards, penetrating each other and continuing afterwards until they reach the ends of the subsystem.

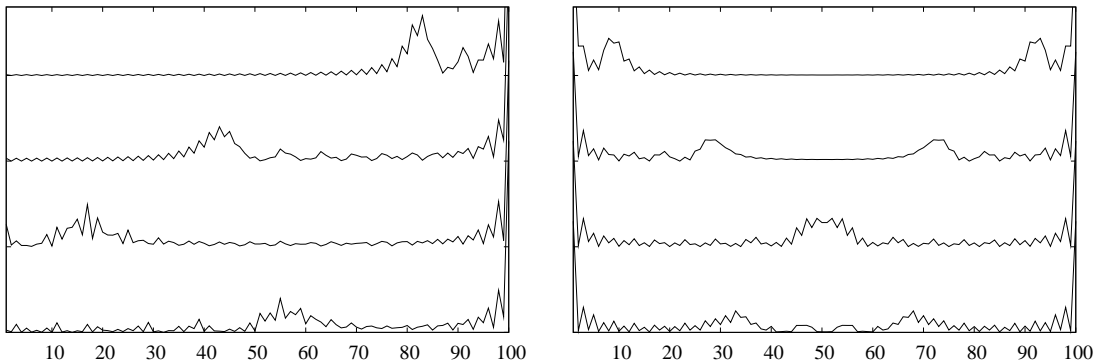


Figure 3. Front propagation in the lowest single-particle eigenvector for $L = 100$, with time increasing from top to bottom. Left: semi-infinite geometry, $t = 20, 60, 120, 160$. Right: infinite geometry, $t = 10, 30, 50, 70$. Shown are the absolute squares of the amplitudes.

The evolution of the single-particle eigenvalues is shown in Fig. 4. The horizontal scale has been chosen in order to make the features at both small and large times clearly visible. The general picture is similar to the one that was found previously for one defect in an infinite system [4]. In the beginning the ε_k drop to some transient values which produce the plateau in $S(t)$ and subsequently they approach their equilibrium values. While this happens fast for the lowest ε_k , considerable deviations remain for long times among the higher ones. These are the “anomalous” eigenvalues. The deviations, however, are stronger than in [4] and there is a new feature in the form of certain

intervals where the eigenvalue is roughly constant before evolving again. We will come back to this phenomenon below.

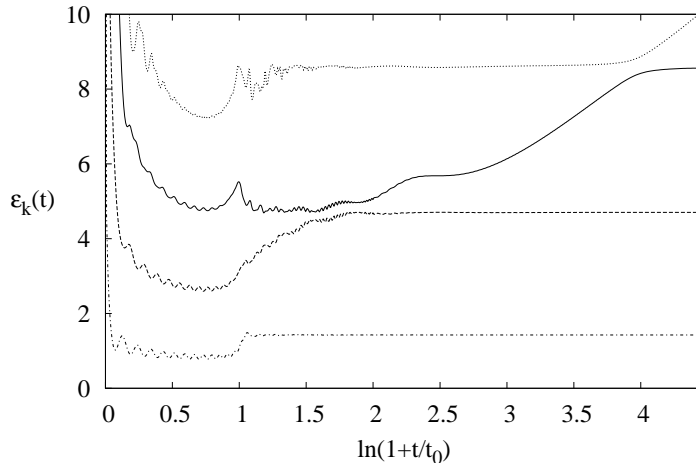


Figure 4. Time evolution of the lowest four single-particle eigenvalues for the semi-infinite geometry with $L = 40$. The parameter t_0 was chosen such that $t = 2L$ gives 1 on the horizontal axis.

Plateau region

For the semi-infinite geometry, Calabrese and Cardy recently derived the following formula for $S(t)$ from conformal field theory [5]

$$S(t) = \frac{c}{6} \ln \left[\frac{4L}{\pi} t \sin \left(\frac{\pi t}{2L} \right) \right] + k'. \quad (12)$$

Here c is the central charge, equal to 1 for the XX model, and the cutoff parameter ε appearing in the calculation has been included in the constant k' . This formula is supposed to be valid as long as the sine remains positive, i.e. for times up to $t = 2L$. The lower curves in Fig. 5 show a comparison of numerical data with this prediction for a system with $L = 60$. There are deviations at the right and left end of the interval and the data shows additional oscillations, but overall the agreement is very good. Leaving the value of c free, a fit between $t = 10$ and $t = 110$ gives $c = 0.993$. Also the dependence on L is described properly, i.e. curves for different L collapse in reduced variables. Thus, in spite of an approximation involved deriving it [5], formula (12) describes the lattice result very well.

The infinite geometry was not treated in [5]. However, as sketched in Appendix B, one can generalize the approach to this case by using an additional conformal mapping. The result after a rather long calculation is

$$S(t) = \frac{c}{3} \ln \left[\frac{2L}{\pi} t \sin \left(\frac{\pi t}{L} \right) \right] + k. \quad (13)$$

Thus, compared to (12), the prefactor has twice its value, which is due to the two points of contact between subsystem and surrounding, and $2L$ has been replaced by L . A

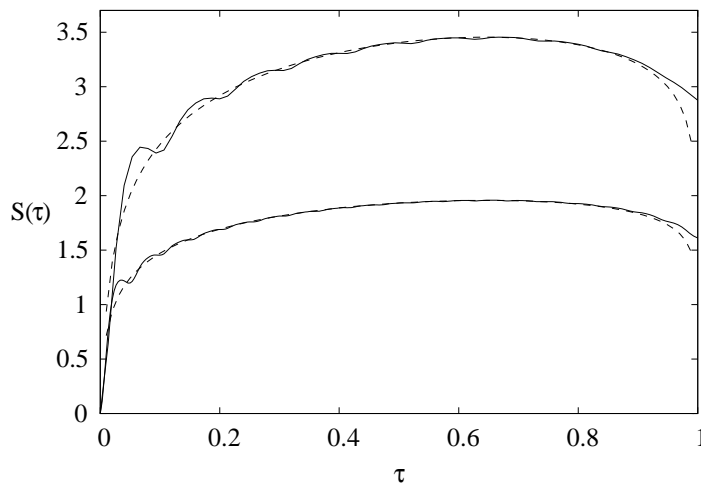


Figure 5. Entropy plateau. Numerical results (solid) and conformal predictions (dashed) for $L = 60$. Upper curves: infinite case, $\tau = t/L$. Lower curves: semi-infinite case, $\tau = t/2L$.

comparison of this formula to the numerical data is given by the upper curves in Fig. 5, again for $L = 60$. The curves look very similar to the lower ones and the agreement is again very good. The same kind of fit as before gives in this case $c = 1.007$

The conformal field theory, which deals with particles of uniform velocity $v = 1$, does not give the oscillations seen in the numerics and the relaxation at long times. Both are lattice effects connected with the dispersion of the elementary excitations in the model.

Long times

The behaviour at long times is more intriguing here than for a single defect in an infinite chain. From Fig. 2 it might seem that $S(t)$ simply decays towards its equilibrium value. Looking closer at the semi-infinite case, however, one finds a clear step structure. This is shown in Fig. 6 for two values of L . These steps become quite regular if one plots S vs. $1/t$ as in the right part of the figure. Their height decreases with L roughly according to a power law $L^{-\alpha}$ where $\alpha \approx 0.90$. A comparison with the single-particle spectrum in Fig. 4 shows that the steps occur for those times where the anomalous eigenvalue has the flat intervals mentioned previously. These are short for the earlier times and longer for the later times which gives the regular structure in $1/t$.

If one examines the eigenvector of the anomalous single-particle state one finds another surprise. For the flat intervals, it becomes remarkably simple. This is shown in Fig. 7 for $L = 60$ and two times related to the third-last and the last plateau, respectively. Plotted are the absolute squares of the amplitudes. These pictures suggest the functional form

$$|\phi(j)|^2 = A \sin^2(qj) \quad ; \quad q = \frac{\pi}{L+1}n, \quad (14)$$

as for a standing wave in the isolated subsystem and the comparison shows that this

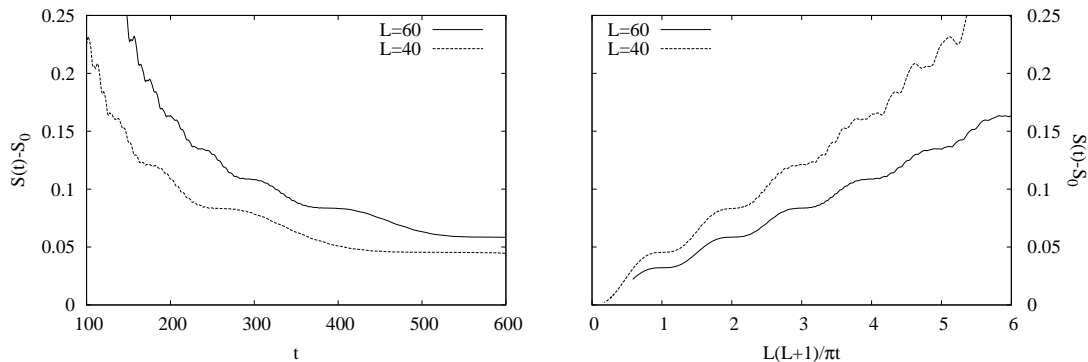


Figure 6. Entanglement entropy at large times for the semi-infinite geometry. Left: S vs. t . Right: S vs. $1/t$. The equilibrium value S_0 is subtracted.

indeed fits the data very well. Moreover, one can take these q -values and calculate the time an excitation with $\omega_q = -\cos q$ created at the initial defect needs to travel through the system. With $v_q = \sin q$ this is

$$T_n = \frac{L}{v_n} \approx \frac{L(L+1)}{\pi n} \quad (15)$$

The times so calculated fit the plateau times in $\varepsilon_k(t)$ resp. $S(t)$ remarkably well. The expression also explains the scale used in the right part of Fig. 6. The plateaus then appear at integer values of the variable.

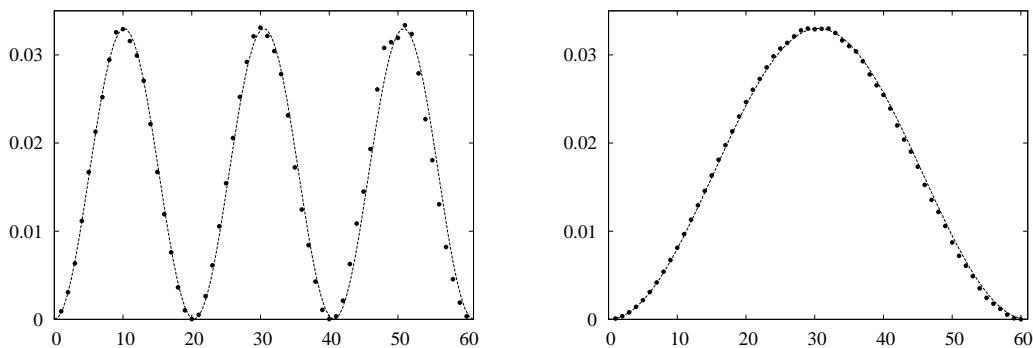


Figure 7. Anomalous single-particle eigenvector for $L = 60$. Left: $t = 390$. Right: $t = 1160$. The dotted lines are fits with the function (14).

Taking all together, one can say that the discrete levels of the isolated subsystem reappear in the time evolution. Since for long times the smallest q -values enter, one is seeing here (in contrast to the fronts discussed earlier) the *slowest* excitations in the subsystem. However, the selection of the q 's is not by interference of a particle with itself, since (15) gives only the time for travelling one way.

All considerations so far were for the semi-infinite case. In the infinite geometry, one also finds such plateaus in the $\varepsilon_k(t)$ at times given by (15) with L replaced with $L/2$. The corresponding eigenvector also has the same features. However, one does

not observe plateaus in $S(t)$, because they are masked by the contribution of another non-constant eigenvalue nearby.

4. Non-critical chains

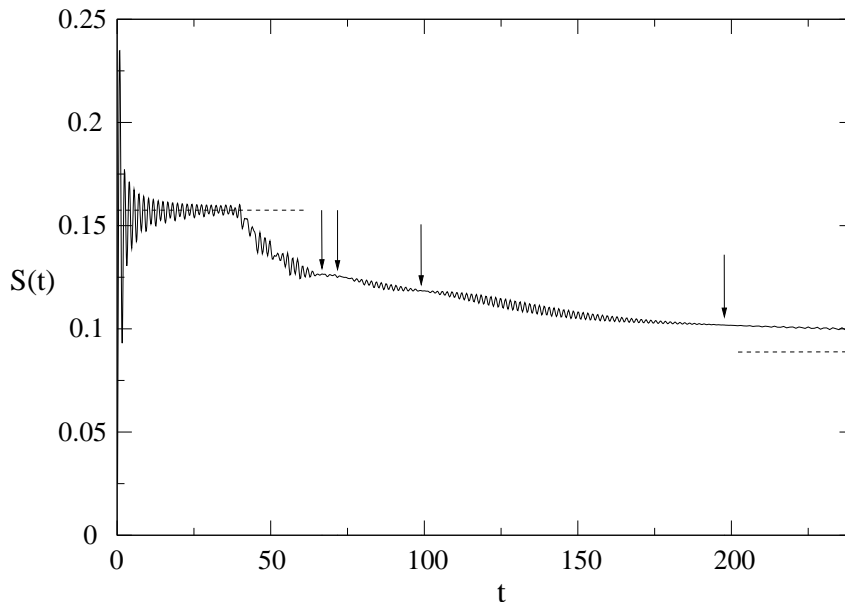


Figure 8. Entanglement entropy for the TI chain in the semi-infinite case with $h = 2$ and $L = 20$. The dashed horizontal lines indicate the plateau value and the equilibrium value, respectively. The arrows give the four longest times $T_n = L/v_n$ defined in the main text.

We now present results for the non-critical TI model in the disordered region $h > 1$. The general behaviour of $S(t)$ is shown in Fig. 8 for the semi-infinite geometry and $L = 20$. This is a relatively small size but still much larger than the correlation length $\xi = (h - 1)^{-1}$ for the chosen value of h . As before, one sees an initial plateau which extends up to $t = 2L$. This is consistent with the velocity of the elementary excitations

$$v_q = h \sin q / \omega_q \quad (16)$$

which gives a maximum value $v = 1$ for $q = \pi/2$ as in the critical case. The height of the plateau is independent of L for $L \gg \xi$ and decreases monotonically as one moves away from the critical point. At the shown value $h = 2$ it is already rather small. Its detailed behaviour can be seen in Fig. 9. One finds numerically that the plateau height is very accurately given by $\sqrt{\pi} S_0$ where $S_0(h)$ is the equilibrium value of the entanglement entropy for large L given analytically in [11]. The relative deviation from this formula is less than 0.1%.

On top of the plateau one sees oscillations as in the critical case. Due to the small plateau height, however, they are more prominent here. They reflect the lattice

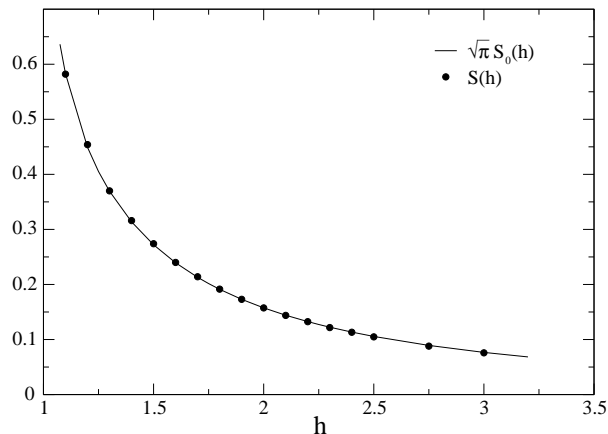


Figure 9. Plateau values of the entanglement entropy as a function of the field h . The line is the equilibrium value $S_0(h)$ multiplied by $\sqrt{\pi}$.

structure of the chain and are shown in more detail on the left side of Fig. 10. Their amplitude decays as $1/t$ while their period changes with the transverse field. From the Fourier spectrum on the right side of the figure one sees that they contain two main frequencies. These are given by $\omega_{\pm} = (h + 1) \pm (h - 1)$ where $h + 1$ and $h - 1$ are respectively the upper and lower band edge of the dispersion curve (3). They would appear in a stationary phase approximation for the integrals in the rotation matrices $\mathbf{R}(t)$ for the time evolution. Of these, the larger frequency $\omega_+ = 2h$ contributes with higher weight. Moreover, there is a peak in the spectrum at zero frequency. Thus, to leading order $S(t)$ in the plateau region is described by the expression

$$S(t) \simeq \sqrt{\pi} S_0(h) + \frac{1}{t} [A + B \cos(2ht)] \quad (17)$$

where A and B are constants depending a priori on L and h .

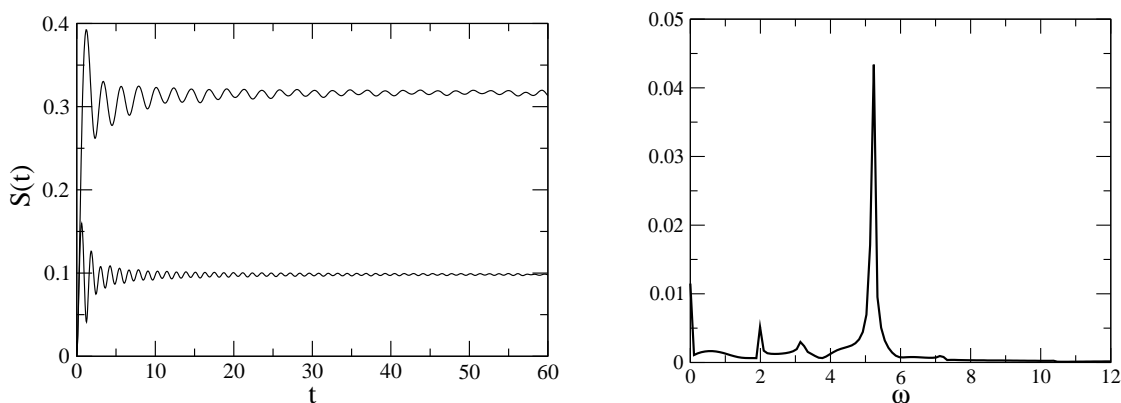


Figure 10. Left: Entanglement entropy in the plateau region for $L = 30$, $h = 1.4$ (top) and $h = 2.6$ (bottom). Right: Power spectrum of $t[S(t) - \sqrt{\pi}S_0]$ for $h = 2.6$. The main peak is located at $\omega = 5.2$.

For times longer than $2L$, Fig. 8 shows a slow decay of the entanglement entropy which is similar to the one in the critical case and the curve seems to approach the

equilibrium value S_0 . If one assumes that, the decay is approximately a power law t^α with an exponent near one. Due to the calculational procedure, the accessible times are smaller here and limited to about 300. In this region, the spectrum of the single-particle eigenvalues still deviates markedly from its asymptotic form. Only the lowest one has the value one finds from the relation to corner transfer matrices [12, 11], namely

$$\varepsilon_1 = \pi I(k')/I(k), \quad k = 1/h, \quad k' = \sqrt{1 - k^2} \quad (18)$$

where $I(k)$ is the complete elliptic integral of the first kind, while the next two are irregular. Thus one cannot check the approach to equilibrium very well. The curve for $S(t)$ shows again certain structures, but these are nodes between oscillatory regions rather than steps. Nevertheless, as can be seen from Fig. 8, they occur at the characteristic times $T_n = L/v_n$ calculated from the velocities (16). The allowed values of q in the non-critical case are not equidistant and lead to different velocities near the upper and lower band edge. Finally, one should note that the overall behaviour of $S(t)$ has a certain universal character, since only one time scale, namely L , enters. Thus one obtains an approximate collapse of the curves for different L (but fixed h) if one plots them as a function of t/L . This means that after times $t > 2L$, the decay is slower for larger subsystems.

5. Summary and discussion

We have studied a special case of a local quench, namely the joining of initially separated parts of a one-dimensional system, all prepared in their ground states. The quantity of interest was the entanglement entropy between a finite piece and the remainder of the chain. We found that S behaves in a similar way as after the removal of a single defect from an infinite system [4]. There is a transient regime where entanglement builds up rapidly and a plateau forms. Its length is determined by the velocity of the fastest particles. In the critical case, its form is given by a universal logarithmic function and follows from conformal field theory. For non-critical chains, it is rather flat and its height varies with the parameters of the system. At later times, there is a slow decay towards the equilibrium entanglement in all cases. Thus one has a kind of overshooting phenomenon.

The critical case turned out to be particularly interesting for the semi-infinite geometry. Then the final decay of S proceeds in a step-like fashion with flat regions determined by the travelling times of the slowest particles in the initially isolated subsystem. Thus, while the gradual descent is generally a consequence of the dispersion in the velocities, it shows here some memory of their initial discreteness. This is connected with a special behaviour of the anomalous single-particle eigenvalues of the reduced density matrix and their eigenvectors. On that level, it seems rather general for this type of quench. However, to be observable in the entanglement entropy, a proper eigenvalue structure is necessary. Although we can describe the phenomenon rather precisely, we have no complete picture of the mechanism. The same holds for the

simple formula giving the plateau height for the TI chain in terms of the equilibrium entanglement.

The physical situation we have addressed, has been considered with a different focus in various other papers. For example, in [13] oppositely magnetized XX half-chains were brought into contact and the interest was in the magnetization profile. In a fermionic picture this corresponds to charge transport via tunnel contacts as studied in [14]. Generalizations include the case of finite temperatures and a sandwich structure corresponding to our infinite geometry [15, 16, 17, 18]. In [19] also the entanglement for large times was considered. However, for finite temperatures the entanglement entropy becomes extensive and does not measure the quantum properties we were studying here. Nevertheless, such an extension can put the zero-temperature features in a broader context.

Acknowledgement

We would like to thank W. Aschbacher, P. Calabrese, J. Cardy, J. Eisert, K. Schönhammer and U. Schollwöck for discussions.

Appendix A: Entanglement in XY and TI chains

As pointed out recently [10], there is a close connection between the ground state entanglement entropy of the zero field XY chain and the TI chain. This was derived by a detailed comparison at the level of the fermionic Hamiltonians and the correlation matrices. Here we extend this to the non-equilibrium case using more general arguments.

It has been known for a long time [20, 21] that the zero field XY Hamiltonian (1) can be split into a sum of two independent TI Hamiltonians by distinguishing even and odd lattice sites and using a dual transformation. If the couplings $(1 \pm \kappa)$ in (1) are denoted by J_x and J_y these are

$$H_{I,1} = -\frac{1}{2} \sum_{i=1}^{N/2-1} J_x \tau_i^{x,1} \tau_{i+1}^{x,1} - \frac{1}{2} \sum_{i=1}^{N/2} J_y \tau_i^{z,1} \quad (19)$$

and

$$H_{I,2} = -\frac{1}{2} \sum_{i=1}^{N/2-1} J_y \tau_i^{x,2} \tau_{i+1}^{x,2} - \frac{1}{2} \sum_{i=1}^{N/2} J_x \tau_i^{z,2} \quad (20)$$

Here the τ operators are related to the σ 's via [10]

$$\begin{aligned} \tau_i^{x,1} &= \prod_{j=1}^{2i-1} \sigma_j^x, & \tau_i^{x,2} &= \prod_{j=1}^{2i-1} \sigma_j^y \\ \tau_i^{z,1} &= \sigma_{2i-1}^y \sigma_{2i}^y, & \tau_i^{z,2} &= \sigma_{2i-1}^x \sigma_{2i}^x \end{aligned} \quad (21)$$

One then has the decomposition

$$H_{XY} = \frac{1}{2} [H_{I,1} + H_{I,2}] \quad (22)$$

with $[H_{I,1}, H_{I,2}] = 0$. If the XY chain is cut at one point, the TI chains are also cut. Therefore, the initial ground state of the XY chain factorizes as

$$\Phi_{XY}(0) = \Phi_{I,1}(0) \Phi_{I,2}(0) = \Phi_{I,1}^1(0) \Phi_{I,1}^2(0) \Phi_{I,2}^1(0) \Phi_{I,2}^2(0). \quad (23)$$

where the superscripts refer to the two subsystems. The evolution operator $U_{XY}(t) = e^{-itH_{XY}}$ factorizes as well, since $[H_{I,1}, H_{I,2}] = 0$

$$U_{XY}(t) = U_{I,1}(t/2) U_{I,2}(t/2) \quad (24)$$

and the state at a later time is given by

$$\Phi_{XY}(t) = \Phi_{I,1}(t/2) \Phi_{I,2}(t/2). \quad (25)$$

Tracing over the unwanted degrees of freedom, one obtains the reduced density matrix as

$$\rho_{XY}(t) = \rho_{I,1}(t/2) \rho_{I,2}(t/2) \quad (26)$$

and, restoring the length L , one has for the entanglement entropy

$$S_{XY}(L, t) = S_{I,1}(L/2, t/2) + S_{I,2}(L/2, t/2). \quad (27)$$

In the isotropic case, i.e. for the XX chain, the two TI models are identical and critical and (27) gives (11) in Section 2.

Appendix B: Conformal mapping

For the semi-infinite chain, the formula (12) was derived in [5] within a path-integral approach for the quantum system. This leads to considering a complex $(x, i\tau)$ plane, where τ is the imaginary time. In this plane, one has a vertical line representing the boundary and a pair of half-infinite vertical lines representing the cut in the chain which exists up to $\pm i\varepsilon$. The entanglement entropy $S(t)$ is obtained from the expectation value of an operator $\Phi_n(i\tau_0)$ in the gap between these half-lines after the analytic continuation $\tau_0 \rightarrow it$. To obtain this expectation value, one first simplifies the geometry by mapping the area to the right of the boundary line, where the path integral is to be taken, onto the right half-plane. As explained in [5], this can be done approximately by the combination of a Joukowski transformation, a reflection at the unit circle and a logarithmic map. The resulting transformation is analytically invertible which is needed for the application of the conformal formulae.

The infinite chain with initially two cuts can be related to this problem in the following way. One has to consider in this case a complex plane with *two* pairs of half-infinite vertical lines and the path integral is taken everywhere. The situation is shown in Fig. 11 on the left. The transformation

$$z' = \frac{1}{2}(\sqrt{z^2 + \varepsilon^2} - z) - L \quad (28)$$

which is a Joukowski transformation as in [5], followed by a reflection, an inversion and a translation by L then maps this approximately onto the shaded region of the

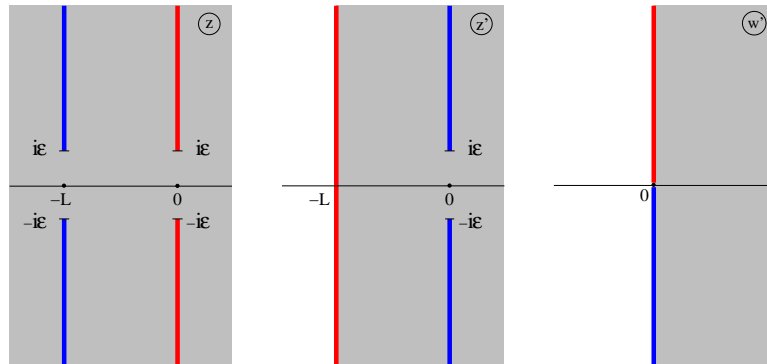


Figure 11. Conformal mapping of the infinite geometry with two cuts (left) to the semi-infinite one with one cut (center) and onto the right half-plane (right). The path integrals are taken in the dark areas. The colours show how the various lines transform.

z' -plane shown in the center of Fig. 11. This is exactly the geometry for the single cut and one can use the previous procedure to map it to the right w' half-plane. The only additional feature is that the entanglement entropy follows here from a two-point function $\langle \Phi_n(i\tau_0)\Phi_n(i\tau_0 - L) \rangle$. From its form in the w' -plane [5]

$$\langle \Phi_n(w'_1)\Phi_n(w'_2) \rangle = c_n^2 \left[\frac{|w'_1 + w'_2|^2}{|w'_1 - w'_2|^2 |2\text{Re}w'_1| |2\text{Re}w'_2|} \right]^{x_n} \quad (29)$$

where $x_n = c(n - 1/n)/12$ one obtains it in the z -plane by the usual conformal transformation formula.

$$\langle \Phi_n(z_1)\Phi_n(z_2) \rangle = \left[\left| \frac{dw'}{dz} \right|_1 \left| \frac{dw'}{dz} \right|_2 \right]^{x_n} \langle \Phi_n(w'_1)\Phi_n(w'_2) \rangle \quad (30)$$

After a lengthy calculation and analytical continuation, assuming $t, L \gg \varepsilon$, this leads to

$$\langle \Phi_n \Phi_n \rangle = c_n^2 \left[\left(\frac{\pi}{2L} \right)^2 \left(\frac{\varepsilon}{t} \right)^2 \frac{1}{\sin^2(\pi t/L)} \right]^{x_n} \quad (31)$$

Here the first two factors in the brackets come from the derivatives dw'/dz while the sine arises from the denominator in (29). The entanglement entropy is the negative derivative with respect to n at $n = 1$ which gives (13) in section 3.

References

- [1] Amico L, Fazio R, Osterloh A and Vedral V 2007 quant-ph/0703044
- [2] Calabrese P and Cardy J L 2005 *J. Stat. Mech.* P04010
- [3] De Chiara G, Montangero S, Calabrese P and Fazio R 2006 *J. Stat. Mech.* P03001
- [4] Eisler V and Peschel I 2007 *J. Stat. Mech.* P06005
- [5] Calabrese P and Cardy J L 2007 *J. Stat. Mech.* P10004
- [6] Lieb E H, Schultz T D and Mattis D C 1961 *Ann. Phys., NY* **16** 406
- [7] Peschel I 2003 *J. Phys. A: Math. Gen.* **36** L205
- [8] Iglói F and Rieger H 2000 *Phys. Rev. Lett.* **85** 3233
- [9] Karevski D 2002 *Eur. Phys. J. B* **27** 147
- [10] Iglói F and Juhász R 2007 arXiv:0709.3927

- [11] Peschel I 2004 *J. Stat. Mech.* P12005
- [12] Peschel I, Kaulke M and Legeza Ö 1999 *Ann. Physik (Leipzig)* **8** 153
- [13] Antal T, Rácz Z, Rákos A and Schütz G M 1999 *Phys. Rev. E* **59** 4912
- [14] Schönhammer K 2007 *Phys. Rev. B* **75** 205329
- [15] Ogata Y 2002 *Phys. Rev. E* **66** 016135
- [16] Aschbacher W H 2006 *Lett. Math. Phys.* **77** 11
- [17] Platini T and Karevski D 2005 *Eur. Phys. J. B* **48** 225
- [18] Platini T and Karevski D 2007 *J. Phys. A* **40** 1711
- [19] Aschbacher W H 2007 *Lett. Math. Phys.* **79** 1
- [20] Peschel I and Schotte K D 1984 *Z. Phys. B* **54** 305
- [21] Turban L 1984 *Physics Letters A* **104** 435